DEM Matching and Detection of Deformation in Close-Range Photogrammetry without Control

Abstract

A method for matching pairs of digital elevation models (DEMs), based on surface shape and without control points, has been evaluated in close-range photogrammetry. Results presented for 30 DEM pairs of the human body trunk and of varying relief indicate that the influence of orientation errors has been effectively removed from the transformed models. The final RMS differences in relief are close to the RMS errors of the elevations themselves. Introduction of gross error detection techniques, such as "data-snooping," simultaneously allows orientation based on similar model regions and localization of deformations. The magnitude of the latter is adequately estimated using the weight cofactor matrix of residuals. Experiments with simulated and actual deformations illuminate the potential of this approach for close-range photogrammetry.

Introduction

Traditionally, the procedure of absolute orientation in photogrammetry is based on control points of known position. However, establishment of control might be costly or in some cases not possible. Orientation based on shape and without control points should instead be considered. For example, for digital elevation models (DEMs) without obvious characteristic points, feature point extraction from DEM elevations based on curvature has been suggested for three-dimensional matching (Goldgof *et al.*, 1989). Rosenholm and Torlegård (1988), on the other hand, have used DEMs as sole information for stereomodel orientation in a modified similarity transformation relying on DEM slopes. Such approaches are, in fact, suitable for several applications of close-range photogrammetry. In this field, digital elevation models are now increasingly used while control is not always available or even possible. Biostereometrics is the specific example considered here.

Photogrammetric methods for automatically identifying points of peculiar curvatures on the human back have been recently reported (e.g., Frobin, 1992). Nevertheless, difficulties in identifying "landmarks" for establishing a reliable body-fixed datum are generally common in medical applications. Furthermore, *a priori* body positioning with position holders yields poor accuracies as compared to the actual precision of the measurements (e.g., Wegner, 1985).

As an alternative to external and internal control, DEMs could be mutually orientated by matching surface shape. Pilgrim (1989) has outlined the advantages of such an approach for medical applications. Using moiré topography, Roger (1980) experimented with a two-step procedure for optimizing DEM overlay by first sliding one surface to recover translation and, subsequently, "self-referencing" DEMs through plane-fitting to recover two rotations. However, the final mismatches reported considerably exceeded the digitization error.

As a rule, a DEM pair in close-range photogrammetric applications will not consist of two identical models. The DEMs to be matched may refer to different time epochs (as in biostereometrics, for instance); or represent a surface to be controlled against a standard (e.g., in the field of industrial applications). Consequently, DEM pairs in close-range photogrammetry are generally to be checked for unsimilarity (i.e., deformation). "Orientation" in this context means in practice both matching of similarities as well as localization of deformation. Thus, the introduction of a technique for gross error detection may constitute an option indispensable for most applications in close-range photogrammetry.

In this paper shape-matching, as applied by Rosenholm and Torlegård (1988) to ground DEMs, is examined in an example of biostereometrics. Results are presented for DEMs of varying slope distributions. The method is subsequently extended with the introduction of the data-snooping technique, leading to the practical detection of deformations. Experimental results are reported. A procedure for improving estimation of deformation size is also suggested.

Matching of Similar DEMs

Mathematical Model

Let $Z = F(X,Y)$ and $Z' = F'(X,Y)$ be two known n by m DEMs of the same surface located close to each other. Elevations Z and Z' correspond to the same planimetric position X,Y but different physical points on the surface. Assume that the two models are brought to coincidence by small translations and rotations of the second DEM. Then the new coordinates X'',Y'',Z'' of the points of the second model can be linearly approximated on the basis of the commonly used differential equations of absolute orientation. These are

$$\begin{aligned} X'' &= X + \Delta X = X + X_o - Y\kappa + Z'\varphi \\ Y'' &= Y + \Delta Y = Y + Y_o + X\kappa - Z'\omega \\ Z'' &= Z' + \Delta Z = Z' + Z_o - X\varphi + Y\omega \end{aligned} \quad (1),$$

X_o, Y_o, Z_o being here small translations and ω, φ, κ small rotations about the respective axes. These six parameters describe the relative orientation of the DEMs. As the two surfaces X,Y,Z and X'',Y'',Z'' are thus assumed to be matched

Photogrammetric Engineering & Remote Sensing, Vol. 59, No. 9, September 1993, pp. 1419–1424.

0099-1112/93/5909–1419$03.00/0

George E. Karras
Elli Petsa
Laboratory of Photogrammetry, National Technical University, 15780 Athens, Greece.

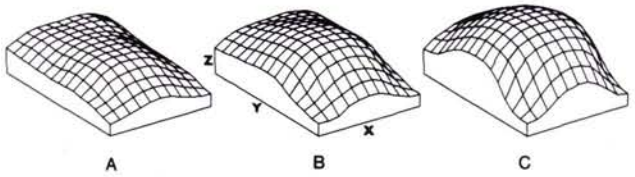

Figure 1. Typical DEMs of slope classes A, B, and C.

TABLE 1. MEAN SLOPE AND PRECISION OF DEMS

Slope Class	Slope°	X-Slope°	Y-Slope°	Digitization and Interpolation Error RMSΔZ (mm)
A	25	20	11	1.1
B	32	24	18	1.3
C	39	30	24	1.5

TABLE 2. RESULTS OF MATCHING OF DEM PAIRS (RMSΔZ IN MM)

Slope Class	Before Matching		After Matching	
	Mean	*Range*	*Mean*	*Range*
A	4.1	1.7–6.7	1.4	0.9–1.8
B	4.2	2.1–8.0	1.5	1.1–1.7
C	5.3	2.8–8.9	1.5	0.7–1.9

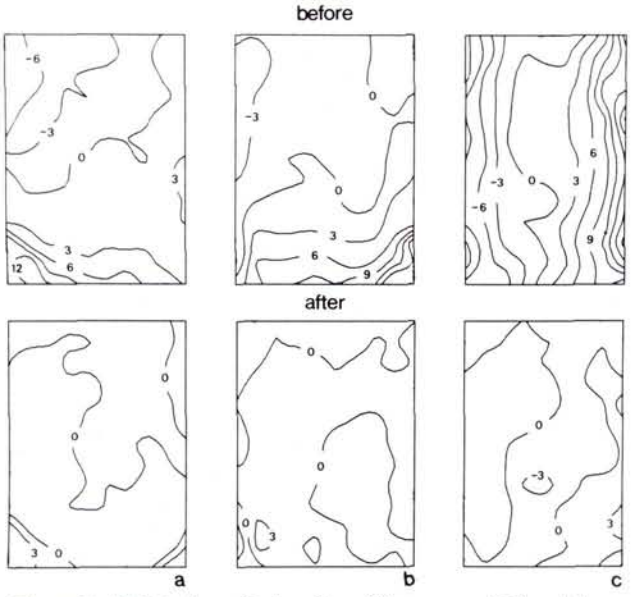

Figure 2. Distribution of elevation differences ΔZ (mm) before and after orientation. Differences above are mainly caused by (a) κ, ω, and Y_o; (b) φ and Y_o; and (c) X_o.

after this rigid body transformation, Z'' could be also approximated on the reference surface F as

$$Z'' = Z + F_X\Delta X + F_Y\Delta Y \qquad (2).$$

F_X, F_Y denote the partial derivatives (i.e., the slopes) of F and ΔX, ΔY are the differential changes in X, Y.

All differences $\delta_i = Z_i - Z'_i$ are introduced as observational quantities into an iterative least-squares adjustment based on Equation 3 resulting from Equations 1 and 2: i.e.,

$$\delta = Z_o - F_X X_o - F_Y Y_o + \kappa(F_X Y - F_Y X) + \omega(Y + F_Y Z') - \varphi(X + F_X Z') \qquad (3).$$

The six orientation parameters are recovered after convergence. A scale parameter may also be included if necessary (Rosenholm and Torlegård, 1988). As F will generally not be continuous, approximations of the slopes over two DEM grid unit lengths are usually used.

After each iteration the points of the second surface are transformed into new coordinate triplets X'', Y'', Z'' by using in Equation 1 the updated orientation parameters. A new DEM $z = f(X,Y)$ is subsequently interpolated from X'', Y'', Z''. The next iteration is based on the new differences $\delta = Z - z$. (For an alternative procedure, see Rosenholm and Torlegård (1988).) Usually, three iterations are sufficient.

Input Data

The contours of 60 moiré topograms of the abdominal area during pregnancy were intially digitized. Body orientation was loosely controlled. All coordinates were transformed into a system based on three poorly defined body landmarks to roughly remove the effect of positioning from the data. DEMs were subsequently interpolated.

Models of three slope classes (A,B,C), corresponding, respectively, to the third, sixth, and ninth months of pregnancy, were selected (Figure 1). Mean slopes are shown in Table 1. Ten DEM pairs were employed for each slope class. Each pair consisted of a DEM of reference and a DEM of the same surface, reconstructed from a different image, which was to be matched with the former. The DEMs were described by 150 to 192 nodes and each covered an area of about 23 by 32 cm² (DEM grid interval about 2.2 cm).

The joint error of digitization/interpolation was estimated by comparing paired DEMs based on images digitized twice. It is expressed as the RMS differences in elevation (RMSΔZ) shown in Table 1. In fact, matching of DEMs aims at reaching these error limits, thus freeing DEM data from the influence of inaccurate orientation.

Orientation Results

The differences in elevation before and after the matching adjustment are seen in Table 2 and illustrated in Figure 2. The RMSΔZ values after matching are very close to the estimated digitization and interpolation errors of Table 1. These results suggest that differences in elevation due to inaccurate relative orientation within DEM pairs, which are responsible for the high RMSΔZ values before matching of Table 2, have been effectively removed after matching.

Indications for the effects of slope are detected in the precision of the unknowns (see Table 3). Planimetric parameters X_o and Y_o, depending exclusively on slopes as seen from Equation 3, are less precise for the "flatter" group A.

Table 4 presents the mean and maximum values of the six orientation parameters. It is seen that, at least for the par-

TABLE 3. OVERALL STANDARD DEVIATIONS OF ORIENTATION PARAMETERS

Slope Class	σ_{X_o} (mm)	σ_{Y_o} (mm)	σ_{Z_o} (mm)	σ_ω°	σ_φ°	σ_κ°
A	0.7	0.8	0.2	0.2	0.5	0.3
B	0.3	0.5	0.2	0.2	0.5	0.3
C	0.2	0.4	0.2	0.2	0.4	0.2

ticular surface types used, the method can recover and correct differences in DEM orientation which are not necessarily small (e.g., rotation angles > 5°).

For several pairs of parameters, correlations proved to be significant. In groups A and B, correlation coefficients ρ were highest for pairs Y_o,ω (mean $\rho = -0.70$) and X_o,φ (mean $\rho = 0.75$). This is apparently why DEM matching using only four parameters (ignoring ω, φ), extracted from the coefficients of best-fitting elliptical paraboloids, gave relatively good results for the same type of surfaces (Karras, 1992).

Grid Interval and Approximation of Slope

Discrete approximations of slope derived from elevations (which again are not error-free) are inevitably inaccurate to a degree depending on surface roughness and DEM grid spacing. Here the topography changed rapidly but smoothly, and approximations over two grid intervals sufficed. Tests with varying grid intervals (1.6 to 3.3 cm) indicated only small improvement with decreasing interval (decrease in RMSΔZ < 15 percent) compared to the computational cost involved.

In order to check the effect of DEM interval on a rougher surface, differently spaced DEMs of a scoliotic back were mathematically rotated and translated. In their new positions, they yielded mismatches of RMS$\Delta Z \approx 5$ mm when compared with their initial positions. Matching was performed both without and with added noise, i.e., perturbation of ΔZ differences by introducing artificial random errors normally distributed about zero. Table 5 shows that, for a rougher surface, matching accuracies depend more strongly on DEM spacing.

Even for unperturbed elevations, matching is not perfect. This is clearly seen in the last three rows of Table 5 where no random errors had been added, i.e. the two DEMs were identical. There, the RMSΔZ values are still not very close to zero. These results refer to DEM matching not influenced by digitization, as the one DEM has been simply created through a rigid transformation of the other. Consequently, the last three rows of Table 5 point at aspects of the inherent accuracy limitations of the method, i.e., regardless of random errors. In general, these limitations are the combined effect of (a) linearization, (b) surface roughness, (c) DEM spacing and (d) successive DEM interpolations.

Detection of Deformation

In close-range photogrammetry the detection of changes between models is often required. If a deformation has to be localized and estimated, sensitive tests applicable to the individual residuals (instead of global statistical tests) are necessary.

The vector **v** of residuals is an indirect expression of the vector **e** of observational (random and gross) errors through the configuration of the adjustment. If no weights are used,

$$\mathbf{v} = -\mathbf{Q}_{vv}\mathbf{e} \tag{4}$$

in which $\mathbf{Q}_{vv}$ is the weight cofactor matrix of residuals. The data-snooping technique assumes the presence of only one gross error and tests the standardized residuals

$$w_i = -v_i/\sigma_{vi} = -v_i/(\sigma_o\sqrt{r_i}) \tag{5}$$

whereby σ_o denotes the precision of observations and $r_i = q_{ii}$ is the i-th diagonal element of $\mathbf{Q}_{vv}$ (always $r_i \leq 1$). Among residuals with $w_i^2 > c^2$, the residual with the largest absolute w-value is most likely attributed to a gross error in the corresponding observation. This observation is excluded from the next iteration. Adjustment is completed when no outlying residuals occur. The critical value c is fixed by the significance level $1 - \alpha_o$ of the test (here $\alpha_o = 0.1$ percent and, accordingly, $c = 3.3$ were used).

TABLE 4. MEAN AND MAXIMUM OF ABSOLUTE VALUES OF THE ORIENTATION PARAMETERS

	X_o (mm)	Y_o (mm)	Z_o (mm)	$\omega°$	$\varphi°$	$\kappa°$
Mean	3.8	4.7	2.0	0.7	1.4	1.2
Max	15.9	22.4	9.6	2.1	9.4	4.4

TABLE 5. EFFECT OF DEM GRID INTERVAL ON MATCHING OF IDENTICAL SURFACES WITH AND WITHOUT PERTURBATION OF ELEVATIONS

Grid Interval (mm)	Standard Deviation of Added Random Errors (mm)	RMSΔZ After Matching (mm)
3.3	1.5	2.8
2.2	1.5	1.9
1.1	1.5	1.2
3.3	–	2.6
2.2	–	0.9
1.1	–	0.7

The redundancy numbers r_i reflect local geometry and describe the part of gross errors e_i revealed in the corresponding residuals. Lower bounds

$$\epsilon_i = \lambda_o\sigma_o/\sqrt{r_i} \tag{6}$$

for gross errors just detectable with a given probability β_o can be computed (Förstner, 1986; Caspary, 1988). In the present application, redundancy numbers were indeed large ($r_i > 0.80$ for all observations) indicating good detectability of gross errors. With $\alpha_o = 0.1$ percent and $\beta_o = 80$ percent, the value $\lambda_o = 4.1$ was fixed. For $r_{max} = 0.99$ and $r_{min} = 0.84$, the least detectable gross errors ranged from $\epsilon_i = 4.1\sigma_o$ to $\epsilon_i = 4.5\sigma_o$. With $\sigma_o = 1.4$ mm, the range of the lower bounds would thus be 5.7 mm to 6.3 mm. If error e_i reaches the lower bound ϵ_i pertaining to the corresponding observation, it will be detected with a probability β_o; α_o is the probability of rejecting a good observation. In the following, a gross error e_i exceeding the lower bound ϵ_i of Equation 6 is characterized as "detectable."

Detection of Simulated Deformation

One DEM of slope class A, perturbed in Z with $\sigma_o = 1.4$ mm, was rotated and translated three times with orientation parameter values of growing magnitude (orientations O1, O2, and O3). Nine gross errors of the same sign were then introduced in the above three DEMs in two patterns: in a 3 by 3 grid area (pattern P1); and, alternatively, at nodes randomly scattered over the models (pattern P2). In each case three different error groups of respective error sizes ($6\sigma_o$ to $10\sigma_o$), ($3.6\sigma_o$ to $6\sigma_o$), ($2.4\sigma_o$ to $4.8\sigma_o$) were alternatively used (error size groups S1, S2, and S3). Groups S2 and S3 included certain errors e not exceeding the corresponding lower bounds ϵ (only eight and three errors out of the nine, respectively, were "detectable"). In group S1, on the contrary, all nine errors were "detectable."

A total of 18 separate gross error detection procedures were carried out, as the 18 DEMs created through the combination of three orientations, two error distribution patterns and three error size groups were matched with the original DEM of reference. In Table 6 O1-P2, for example, represents the DEMs resulting from the DEM of reference through orientation O1 and deformed with errors of the distribution pattern P2.

TABLE 6. DETECTION OF NINE SIMULATED GROSS ERRORS

Number of Detected Errors (Redundancy Numbers r = 0.90 − 0.98; σ_o = 1.4 mm)			
Error Group	S1	S2	S3
Error Size (mm)	8.4–14.0	5.0–8.4	3.4–6.7
Total Number of Errors	9	9	9
"Detectable" Errors	9	8	3
Case 01-P1	9	8	3
Case 02-P1	9	9*	0
Case 03-P1	9	8	0
Case 01-P2	9	8	6*
Case 02-P2	9	7	3
Case 03-P2	9	8	4*

01, 02, 03 : Orientations with parameters of growing magnitude.
P1 : Nine gross errors distributed in a 3 by 3 grid pattern.
P2 : Nine gross errors randomly scattered over the DEMs.
* More errors are detected than were "detectable."

TABLE 7. DETECTION OF N BY N SIMULATED GROSS ERRORS

Number of Errors "Detectable"/Detected				
	Total Number of Errors	Error Group S1	S2	S3
Error Pattern 3 by 3	9	9/9	8/8	3/2
Error Pattern 4 by 4	16	16/16	13/0	3/0
Error Pattern 5 by 5	25	25/13	21/3	6/2

Results shown in Table 6 indicate good detectability for the larger errors (groups S1, S2). Problems are mainly encountered with the errors of S3 which, being small, are in part confused with random errors (cases O2-P1, O3-P1).

The initial relative position of DEMs also appears to play a role. Larger values of the orientation parameters (cases involving O2 and O3 in Table 6) seem more flexible (compared to cases involving O1) in absorbing small errors, thus masking their presence (see last column of Table 6).

Detection of gross errors also appears to be sensitive to their spatial distribution pattern. Errors grouped close together (see cases involving P1), as expected when studying deformations, appear as more likely to remain undetected compared to isolated outliers (cases involving P2). This is indicated in the last column of Table 6. It is also noted that in Table 6 there are instances where more errors have been in fact correctly detected than were "detectable" (expected to be detected at the set probability level).

In the case of gross errors grouped tightly together, the area they cover is also important. The larger orientation parameters (orientation O3) were used in a simulation with gross errors alternatively introduced in a 3 by 3, a 4 by 4, and a 5 by 5 grid pattern at one corner of the DEM. All three error groups (S1, S2, S3) were again used. Results for the nine error detection procedures are given in Table 7. They indicate that the detectability of gross errors is affected by their total number. The more extended a deformation, the more likely it seems that it can be "absorbed" in the adjustment. Even for error group S1, in which the smallest error is by 30 percent larger than the corresponding least detectable value, only half of the gross errors were identified in the 5 by 5 case.

Estimation of Deformation

In studies of deformation, its detection may not suffice. Its actual size is also crucial. Due to the singularity of $\mathbf{Q}_{vv}$, the observational errors cannot be extracted using Equation 4. Assuming the presence of only one gross error in each iteration or diagonal prominence in $\mathbf{Q}_{vv}$, error size is estimated, according to Förstner (1986), through Equation 4 as follows:

$$e_i = -v_i/r_i. \tag{7}$$

Ignoring random errors also inherent in the residuals, the accuracy of such estimates can be assessed here by their differences $\Delta e_i = e_i$ (true) $- e_i$ (estimated) from the known artificial gross errors. Correct estimation should yield a mean of Δe_i differences close to zero.

Despite the marked diagonal prominence of $\mathbf{Q}_{vv}$, the means of the Δe_i sets were close to zero only for isolated gross errors (case of pattern P2 used in Table 6). On the contrary, the means of the Δe_i sets for errors spatially close to each other (case of pattern P1 used in Table 6) displayed a mean systematic deviation from zero of about 20 percent. In the latter case, error estimates were not accurate. This is due to correlations among residuals being stronger for neighboring DEM nodes. This means, according to Equation 4, stronger dependence of residuals v_i on errors e_j ($i \neq j$). Furthermore, the more the gross errors, the more off-diagonal elements of $\mathbf{Q}_{vv}$ are involved in "spreading" them over the residuals.

This problem is more pronounced at the DEM corners. There, redundancy numbers are smallest (these observations contribute more to the determination of unknowns) and correlations among residuals are highest. In case (4 by 4)-S1 of Table 7, for example, the mean of relative differences $\Delta e_i/e_i$ of true and estimated gross errors was as large as 32 percent. As gross errors caused by spatially localized deformation are expected to have the same sign, their effects are additive. The use of Equation 7 takes no account of these complications, i.e., the effects of gross errors not known in advance and revealed in subsequent steps.

Improved results can be obtained by multiple outlier testing where the estimates of the errors previously localized are updated at each step (Kok, 1984). For standard data-snooping, an improved error estimation suggested here proceeds as follows. The equation resulting from Equation 4,

$$v_i = -\boldsymbol{q}_i \boldsymbol{e} \tag{8}$$

expresses the i-th residual as the product of $\boldsymbol{q}_i$, denoting the i-th row of $\mathbf{Q}_{vv}$, with the error vector. After all errors have been detected, the ultimate error localized can be estimated directly from Equation 7 because no further gross errors are assumed in the data. All other errors e_k detected previously can then be estimated through Equation 8, one by one all the way back to the one detected first, as

$$e_k = -(v_k + \Sigma q_{jk} e_j)/r_k \tag{9}$$

where e_j stands for all errors localized by data-snooping after e_k and estimated from Equation 9 before it.

For errors grouped together, this procedure improved gross error estimation considerably compared to the use of Equation 7. In the above-mentioned examples, the mean of relative differences $\Delta e_i/e_i$ fell from 20 percent to 4 percent (cases P1 used in Table 6) and from 32 percent to 6 percent in case (4 by 4)-S1 of Table 7.

Experimental Detection of Shape Changes

Three DEM pairs of slope class A, affected by different amounts and types of deformation, were chosen to test the method experimentally. The mean RMSΔZ = 1.4 mm for group A (Table 2) was used as σ_o in data-snooping.

CASE 1. In one image of this pair the body was strongly

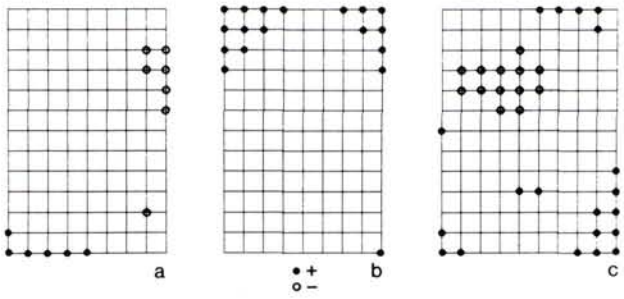

Figure 3. Detected DEM deformations due to (a) torsion of the trunk, (b) different positions of hands, and (c) breathing.

tilted about its vertical axis ($\varphi > 20°$). The DEMs showed a large difference of RMSΔZ = 2.5 mm after matching based on all points (cf. the values for A after matching in Table 2). It was suspected that large body tilts may possibly be spontaneously accompanied by slight torsions of the trunk. The pattern of detected errors in fact indicated such a deformation (Figure 3a). The parameter most affected by this deformation was φ which changed by 2.2° during error detection. DEM matching was satisfactory after the exclusion of deformed points (RMSΔZ = 1.6 mm).

CASE 2. This deformation was due to the arms being stretched once sidewards and once upwards (RMSΔZ = 2.9 mm after matching based on all points). Changes were expected mainly around the upper DEM corners. The pattern of Figure 3b is in agreement with such an assumption (RMSΔZ = 1.7 mm after excluding outliers). Parameters ω and Y_o were strongly affected by the exclusion of deformed points; they changed by 2.7° and 8.0 mm, respectively. Deformation estimates from Equations 7 and 9 differed on the average by 18 percent. Correction of the deformed elevations by means of Equation 9, rather than their exclusion from the adjustment, also gave RMSΔZ = 1.7 mm over the whole DEM. These estimates of Equation 9 are considered as more accurate than those from Equation 7 because, for the latter, it was RMSΔZ = 2.0 mm after correction of the deformed elevations.

CASE 3. Contrary to the above spatially localized deformations, this pair suffered from a deformation spread over the whole model as the DEMs were reconstructed from images taken at different phases of the respiration cycle. Matching using all nodes gave RMSΔZ = 2.8 mm. Roger (1980) has pointed out in this context that, when unsimilarity is present, satisfaction of the least-squares criterion means that differing surface patches are brought closer together while closely fitting ones are moved farther apart. One of the models was "flatter" than the other due to breathing. This was reflected in the parameter value Z_o = 18 mm which is unexpectedly large compared with the Z_o-values of Table 4, i.e., the DEM was shifted considerably in Z to optimize matching. Error detection (which gave RMSΔZ = 2.2 mm) has revealed the deformation of Figure 3c which is not easily explained. This very large value of Z_o, furthermore, did not decrease — as expected — throughout the error detection procedure. This apparently indicates that the two models are essentially different, i.e., that matching still remains "artificial." Thus, the "gross errors" detected are not to be necessarily regarded as the actual deformation but rather as simple statistical outliers within this particular least-squares fit.

Global tests on the *a posteriori* estimations of σ_o related directly to data-snooping are not recommended here as redundancy is large (high risk level of the test) and the true value σ_o is not known. In general, it seems more meaningful to regard data as free of further gross errors if the final values of RMSΔZ fall within the actual RMSΔZ range after matching of Table 2 (i.e., RMSΔZ < 1.8 mm) which has been estimated for pairs of similar DEMs. This was true for Cases 1 and 2 above. In Case 3, the final mismatch of RMSΔZ = 2.2 mm obtained after error detection suggests that the fit still remains problematic.

Conclusion and Discussion

For the particular surface types used, matching without control points was demonstrated to be of good performance. Model pairs are freed from the influences of faulty mutual orientation, and matching accuracies are very close to the limits of digitization and interpolation errors. For the cases studied, slopes were very large (however, Rosenholm and Torlegård (1988) point out that this is often the case in close-range photogrammetry) and surface shape was near-regular. Further experiments are necessary with models of smaller relief, more irregular topography, and varying DEM dimensions.

The method discussed lends itself to the introduction of techniques which allow the localization of deformation. Experiments with one-dimensional data-snooping indicated that it could efficiently detect deformation. Detection of spatially localized deformations, however, appears to be more complicated than detection of isolated outliers. The last example (Case 3 above) also bears witness to a danger that, in cases of extended deformations, "blind" numerical manipulation might be misleading. In fact, it might allow a misinterpretation of actual unsimilarity between models as owing to differences in orientation. This important aspect requires further investigation.

In all experiments presented here, redundancy numbers were large. Thus, the effects of the configuration of the adjustment, represented by r_i in Equation 5, could have been possibly neglected in the tests. In this sense, the identification of a residual v_i as outlying, e.g., simply if $|v_i| > 3\sigma_o$ (an approximate test often used in practice) could probably lead to similar results. This aspect remains to be investigated. However, data-snooping is more sensitive, especially for redundancies distributed less favorably.

Estimates of deformation from Equation 7 appear as rather insensitive to the facts that spatially localized deformations of the same sign are generally expected; and that the neighboring residuals are more strongly inter-correlated. Thus, residuals may be considerably affected by more than one gross error, even if error detectability is good in itself (i.e., large redundancy numbers). This dependence of residuals is taken into account in Equation 9 used in this study for the estimation of error size.

The approach introduced here for DEM orientation with the simultaneous detection/estimation of deformation seems suitable for various tasks of close-range photogrammetry (Rosenholm and Torlegård, 1988; Pilgrim, 1989). In some of these cases, it could be employed in an interactive mode; for other applications, further development would allow an integration of this method in fully automated and real-time environments.

References

Caspary, W.F., 1988. *Concepts of Network and Deformation Analysis.* Monograph 11, School of Surveying, The University of New South Wales, Kensington, 183 p.

Förstner, W., 1986. Reliability, Gross Error Detection and Self-calibration. ISPRS Commission III Tutorial on Statistical Concepts for Quality Control, *International Archives of Photogrammetry*, 26(3/4)1, 34 p.

Frobin, W., 1992. Accuracy of localization of anatomical landmarks from raster-stereographic measurements. *Surface Topography and Spinal Deformity* (A. Alberti, B. Drerup, and E. Hierholzer, editors), G. Fischer Verlag, Stuttgart, pp. 47–51.

Goldgof, D. B., T. S. Huang, and H. Lee, 1989. A curvature-based approach to terrain recognition. *IEEE PAMI* - 11(11):1213–1217.

Karras, G. E., 1992. On the orientation of digital elevation models in biostereometrics. *Surface Topography and Spinal Deformity* (A. Alberti, B. Drerup, and E. Hierholzer, editors), G. Fischer Verlag, Stuttgart, pp. 162–165.

Kok, J.J., 1984. *On Data Snooping and Multiple Outlier Testing.* NOAA Technical Report NOS NGS 30, Rockville, Maryland, 61 p.

Pilgrim, L. J., 1989. Detection of change in 3-dimensional models with time - the medical application, *Biostereometrics '88, Proc. SPIE* (J. U. Baumann and R. E. Herron, editors), 1030:130–137.

Roger, R. E., 1980. *Shape Measurement with Moiré Topography.* Ph.D. Thesis, Department of Engineering Science, University of Oxford, 312 p.

Rosenholm, D., and K. Torlegrd, 1988. Three-dimensional absolute orientation of stereo models using digital elevation models. *Photogrammetric Engineering & Remote Sensing*, 54(10):1385–1389.

Wegner, J., 1985. *Measurement of Scoliosis Deformity Using Moiré Topography.* M.Sc. Thesis, Department of Mechanical Engineering, University of Alberta, Edmonton, 116 p.

(Received 7 August 1991; revised and accepted 6 October 1992; revised 17 November 1992)